www.ThePharmaJournal.com

The Pharma Innovation

ISSN (E): 2277- 7695
ISSN (P): 2349-8242
NAAS Rating: 5.03
TPI 2018; 7(1): 553-560

www.thepharmajournal.com
Received: 22-11-2017
Accepted: 23-12-2017

Sheetal
Department of Chemistry, Maharshi Dayanand University, Rohtak, Haryana, India

SP Khatkar
Department of Chemistry, Maharshi Dayanand University, Rohtak, Haryana, India

VB Taxak
Department of Chemistry, Maharshi Dayanand University, Rohtak, Haryana, India

Sonika Singh
Department of Chemistry, Maharshi Dayanand University, Rohtak, Haryana, India

Correspondence
Sonika Singh
Department of Chemistry, Maharshi Dayanand University, Rohtak, Haryana, India

White light emission of nanocrystalline $La_{1-x}Dy_xSrAl_3O_7$ phosphor via low temperature combustion process

Sheetal, SP Khatkar, VB Taxak and Sonika Singh

Abstract
Nanocrystalline $La_{1-x}Dy_xSrAl_3O_7$ phosphor has been successfully synthesized via low temperature urea assisted solution combustion route. X-ray diffraction (XRD), scanning electron microscopy (SEM), transmission electron microscopy (TEM) and Fourier transform infra-red spectroscopy were used to characterize structural properties of Dy^{3+} doped $LaSrAl_3O_7$ nanophosphor. The results of XRD patterns indicate that all samples crystallized completely in tetragonal phase at sintering temperature 550 ^oC. The functional melilite AlO_4^{5-} groups in $LaSrAl_3O_7$ host were identified using FT-IR spectrum. SEM and TEM analysis revealed tetragonal shaped particles with an average size in the range 65-75 nm. Optical properties were investigated by measuring excitation and emission spectra with decay curves of $La_{1-x}Dy_xSrAl_3O_7$ nanophosphors. Emission spectrum exhibits characteristic blue (479 nm) and yellow emission (574 nm) corresponding to $^4F_{9/2} \rightarrow {}^6H_{15/2}$ and $^4F_{9/2} \rightarrow {}^6H_{13/2}$ transitions of Dy^{3+} ions, respectively under excitation at 352 nm. Luminescence concentration quenching could be observed when the doping concentration of Dy^{3+} ions was more than 10 mol%. The CIE color coordinates (x = 0.332, y = 0.354) located in the white light region, makes this nanophosphor as potential candidate in new lighting devices.

Keywords: Nanophosphor, Combustion, Optical, $LaSrAl_3O_7$

Introduction
Luminescent materials are extremely attractive for both fundamental research and various technological applications including solid state lighting, ionizing radiations, photonics, imaging, and biological assays [1-3]. Optical, electronic and chemical properties of these materials are size dependent and well known to be uniquely different in the "nano-regime" from that in the bulk [4-5]. In rare earth ions (RE^{3+}) based luminescent nanomaterials, doping is significantly important as they exhibit high color purity flexible emission lines with different activators due to their intra 4*f* transitions [6-7]. The optical characteristics of these materials generally depend on the symmetry of local environment of RE^{3+}, spin-orbit coupling of 4f electrons and crystal field effects in the host lattice [8-9]. In rare earth family, Dy^{3+} ions show intense luminescence in blue and yellow spectral region due to transition from $^4F_{9/2}$ energy level to $^6H_{15/2}$ and $^6H_{13/2}$ level, respectively. By suitably adjusting the relative yellow to blue intensities ratios, Dy^{3+} doped nanophosphors may be potentially used for development of white light emission [10-13]. Over the last decade, as RE^{3+} doped luminescent host materials, melilite oxides, ABC_3O_7 (A= Ca, Sr, Ba; B= Y, La, Gd; C = Al, Ga) which can accept high dopant contents and show efficient emission spectra suitable for high resolution optical display systems have been considerably envisioned [14-22]. These oxides possess tetragonal crystal structure with the space group $P\text{-}42_1m$; made up of tetrahedral layered CO_4^{5-} units and eight coordinated A^{2+} and B^{3+} ions having C_s symmetry, randomly distributed in between the layers [23-25].

For the nanocrystalline phosphors with optimized brightness, the prime area concerned are stoichiometry, composition and surface chemistry as lattice defects that acts as non-radiative relaxation channels and quenching sites may degrades the luminescence efficiency [26]. Solution combustion synthesis (SCS) has opened new vistas for the synthesis of highly pure powders having homogeneous and fine particles with large surface area at low temperature in a very short duration as compared to other conventional methods where impurity phase co-exists in the products of same compositions even after long sintering time due to insufficient mixing and low reactivity of raw materials [17-20].

$LaSrAl_3O_7$ is one of the low cost melilite phosphor that could be easily synthesized like other family members using simple and rapid solution combustion approach. This melilite oxide seems to be an ideal host for doping of RE^{3+} ions due to its stable structural features, indicated by recent investigations on luminescent properties of well crystallized Eu/Tb doped $LaSrAl_3O_7$ using SCS and citrate assisted sol-gel method [16-17]. However, to the best of our knowledge, there is no study on the optical properties of Dy^{3+} ions in lanthanum strontium aluminate, $LaSrAl_3O_7$. In the present work, herein we proposed the first time report on the doping of dysprosium ions in melilite oxide, $LaSrAl_3O_7$ via low temperature solution combustion synthesis and studied its structural, morphological and optical features by means of XRD, SEM, TEM, FT-IR and luminescent spectra along with decay curves.

Experimental Details

Powder synthesis

$La_{1-x}SrAl_3O_7$: xDy^{3+} nanopowders, where x = 1 to 15 mol% were synthesized by urea assisted solution combustion process using high purity $Sr(NO_3)_2$, $La(NO_3)_3.6H_2O$, $Al(NO_3)_3$, $Dy(NO_3)_3.6H_2O$ and urea as starting materials. The chemical reaction was:

$1\text{-}xLa(NO_3)_3 + xDy(NO_3)_3 + Sr(NO_3)_2 + 3Al(NO_3)_3 + 11.66CH_4N_2O \rightarrow La_{1-x}Dy_xSrAl_3O_7(s)$ + gaseous products.

According to nominal composition of $La_{1-x}Dy_xSrAl_3O_7$, a stoichiometric amount of metal nitrates were dissolved in minimum quantity of deionized water and then urea was added as fuel. The amount of urea was calculated using total oxidizing and reducing valencies according to the concept used in propellant chemistry [27]. Finally the beaker containing the aqueous paste was placed in a preheated furnace maintained at 500 ºC. The homogenous solution of different oxidizers (metal nitrates) and fuel (urea) undergo rapid and self-sustaining combustion process and the chemical energy released during this exothermic redox reaction results in dehydration and foaming followed by decomposition. Consequently, the large amounts of volatile combustible gases generated alongwith flames, yields voluminous solid within 5-8 minutes. The product thus obtained was again sintered at 550 ºC for 1h in order to eliminate unreacted nitrates, resulting in pure phased $LaSrAl_3O_7$: Dy^{3+} nanophosphor.

Powder characterization techniques

X-ray diffraction (XRD) was performed on the Rigaku Ultima-IV X-ray powder diffractometer using CuKα radiation in the 2θ range of 15-70º. The accelerating voltage and current were at 40 kV and 40 mA. Fourier transform infra-red (FT-IR) spectroscopy was carried out on Perkin-Elmer spectrometer using KBr pellet technique in the spectral range 4000-400 cm^{-1}. The morphology and particle size were inspected using scanning electron microscope, Jeol JSM-6510 and transmission electron microscope, Hitachi F-7500. The photoluminescence excitation and emission spectra in the ultraviolet-visible region and decay curves under time scan-mode were obtained on Hitachi F-7000 spectrofluorimeter equipped with Xe-lamp as the excitation source.

Results and Discussion

$LaSrAl_3O_7$ belongs to the melilite oxide family and composed of AlO_4^{5-} tetrahedral layers with randomly distributed Sr^{2+} and La^{3+} ions having C_s symmetry sites in between the layers. This melilite host comprises of tetragonal crystals with the space group P-42$_1$m and lattice parameter a = 7.890Aº and c = 5.228Aº. The XRD patterns of as-synthesized (500 ºC) and sintered (550 ºC, 1h) sample of $La_{0.90}Dy_{0.10}SrAl_3O_7$ nanophosphor along with standard data of $LaSrAl_3O_7$ (JCPDS No. 50-1815) are depicted in Fig.1.

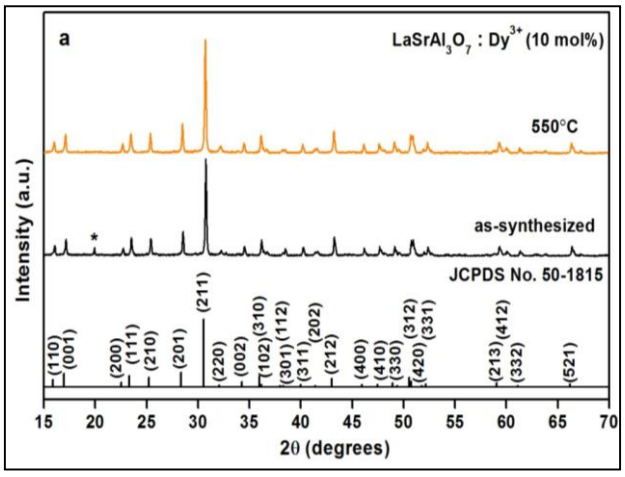

Fig 1: XRD patterns of $La_{0.90}Dy_{0.10}SrAl_3O_7$ nanophosphor as-synthesized (500 ºC) and sintered (550 ºC, 1h) along with standard data of $LaSrAl_3O_7$ (JCPDS No. 50-1815).

The sharp diffraction peaks of as-synthesized $La_{0.90}Dy_{0.10}SrAl_3O_7$ sample are well indexed to tetragonal melilite phase belonging to JCPDS No. 50-1815, indicating that highly crystalline powders has been formed at 500 ºC. It implies that SCS provides the conditions of crystallization through molecular level mixing of the precursors due to self sustained combustion of oxidizers and urea at low temperature (500 ºC). Minor peak at 19.8˚ can be assigned to nitrates residues in the as-synthesized sample although no traces of RE^{3+} ions were noticed indicating complete incorporation of dysprosium ions into the $LaSrAl_3O_7$ lattice. On sintering the powders at 550 ºC for 1h, crystalline degree of the products is improved apparently as peaks pertaining to unreacted nitrate phase disappeared completely although the tetragonal melilite phase is formed even without sintering.

The XRD profiles of $La_{1-x}Dy_xSrAl_3O_7$ (x = 1 to 15 mol%) nanophosphors doped with different Dy^{3+} ions concentration, sintered at 550 ºC alongwith standard reference data (JCPDS No. 50-1815) are presented in Fig. 2. It can been clearly seen that all the samples are well consistent with standard data of tetragonal $LaSrAl_3O_7$ phase having space group P-42$_1$m belonging to JCPDS No. 50-1815.

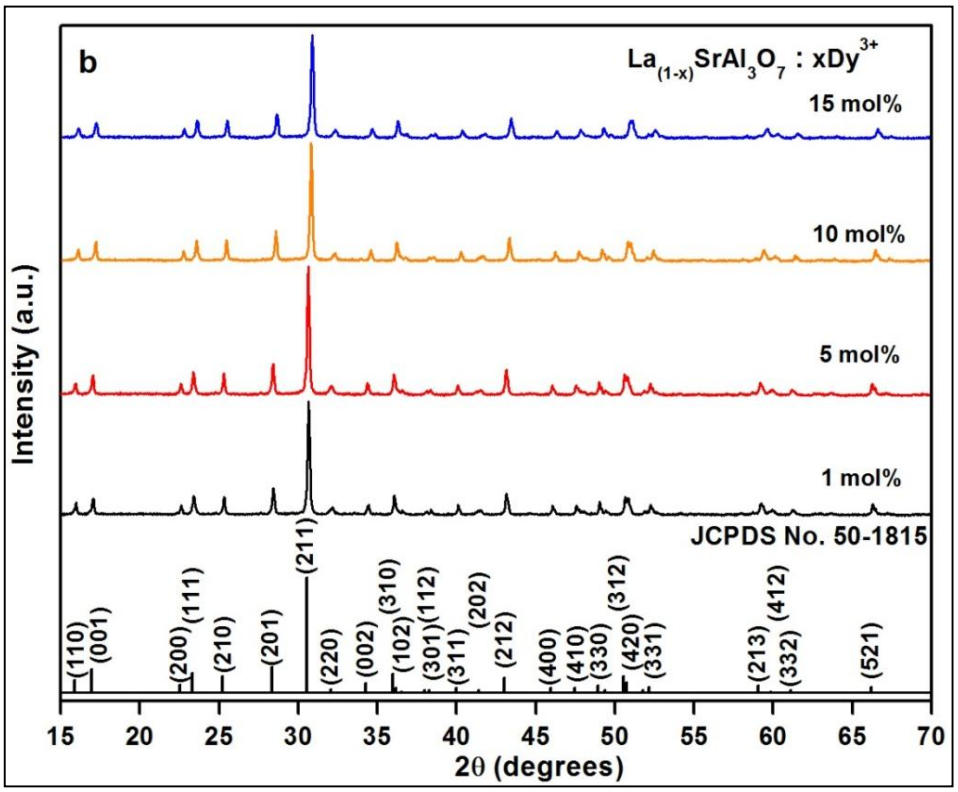

Fig 2: XRD profiles of $La_{1-x}Dy_xSrAl_3O_7$ (x = 1 to 15 mol%) nanophosphors doped with different Dy^{3+} ions concentration, sintered at 550 ºC alongwith standard reference data (JCPDS No. 50-1815).

The well defined diffraction peaks of all samples confirmed that $La_{1-x}Dy_xSrAl_3O_7$ powders maintain the pure tetragonal structure with little variation in dysprosium contents. As expected, Dy^{3+} ions (0.97 Aº) preferentially substitute C_s symmetry sites of La^{3+} ions (1.16 Aº) rather than Sr^{2+} sites (1.26Aº) in $LaSrAl_3O_7$ lattice, on considering the valence states and ionic radii difference. The average particle size, D for $La_{1-x}Dy_xSrAl_3O_7$ powders, was evaluated from the full width half maxima of the most intense diffraction peak according to Scherrer's equation $D = 0.941\lambda/\beta \cos\theta$, where λ is the wavelength of CuKα radiation (0.1548 nm), β is the full width in radians at half-maximum (FWHM) and θ is the Bragg's angle of an observed X-ray diffraction peak. The values of particle size calculated from their corresponding FWHM and diffraction angle (2θ) for 1, 5, 10 and 15 mol% of Dy^{3+} ions in $La_{1-x}SrAl_3O_7$ powder, sintered at 550 ºC were found to be 65 nm, 69 nm, 72 nm and 74 nm, respectively.

SEM image and TEM image of $La_{0.90}Dy_{0.10}SrAl_3O_7$ nanophosphor, sintered at 550 ºC are shown in Fig. 3 and 4, respectively.

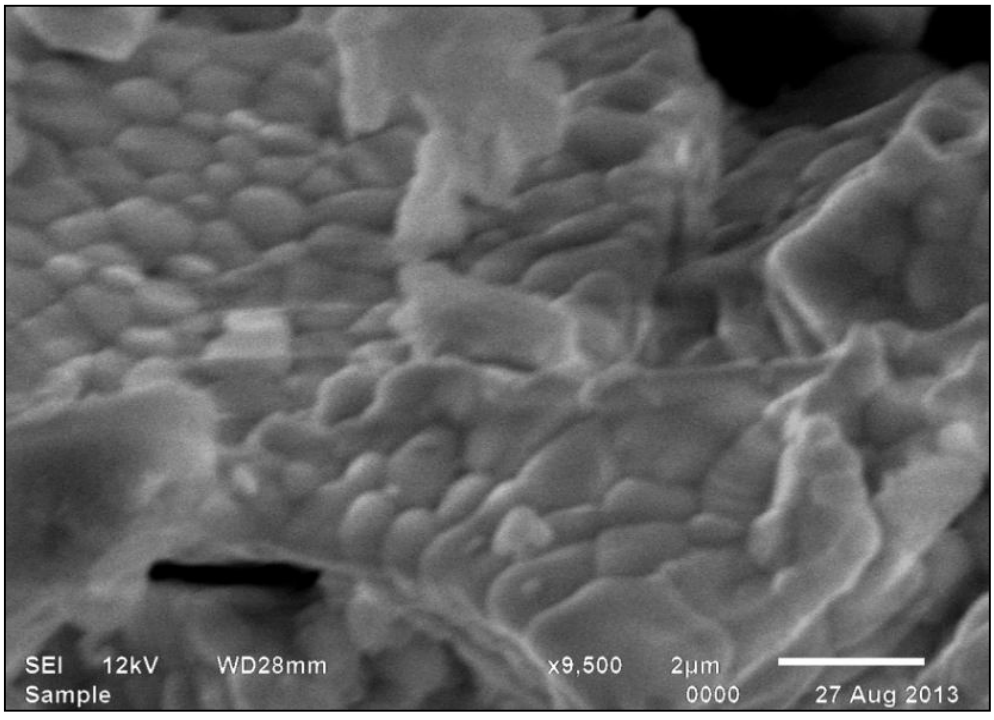

Fig 3: SEM image of $La_{0.90}Dy_{0.10}SrAl_3O_7$ nanophosphor, sintered at 550 ºC.

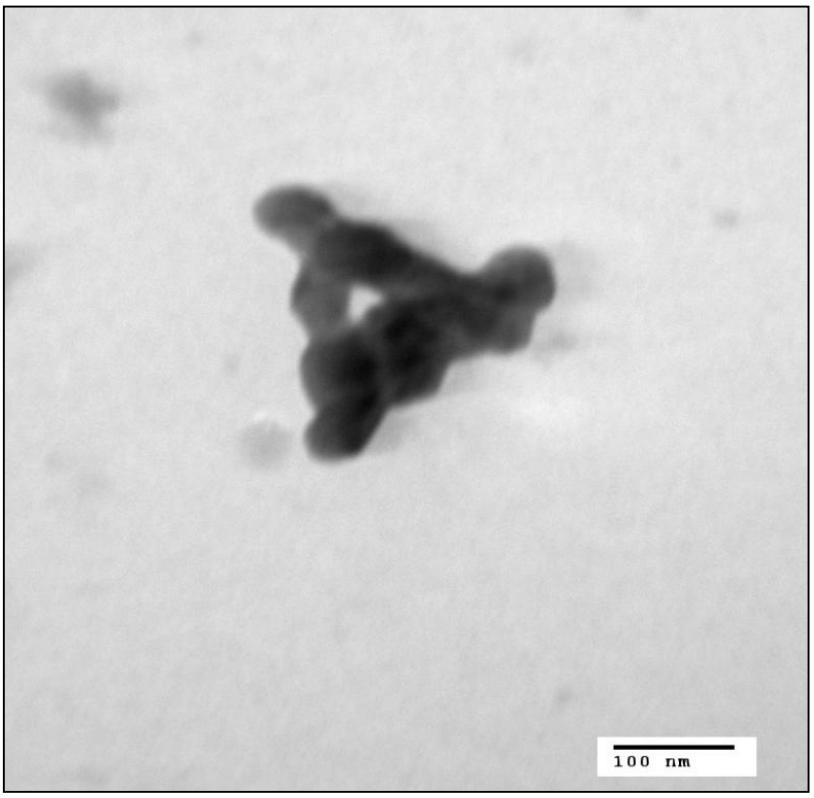

Fig 4: TEM image of $La_{0.90}Dy_{0.10}SrAl_3O_7$ nanophosphor, sintered at 550 ºC.

SEM image displays smooth loosely aggregated tetragonal particles which are packed together by edge-to-edge conjunctions, resulting in high surface area. Due to uncontrolled dynamics of solution combustion process several pores are also apparent on the surface alongwith small particles formed by escaping of large gaseous materials with high pressure. These combustion synthesized powders with high surface area and porous network are highly favorable for better luminescence [20]. TEM image reveals aggregated tetragonal shaped particles with average size ranging between 65 nm and 75 nm. The average particles size estimation nanophosphor was found to be consistent with that determined using Scherrer's equation. Figure 5 shows the FT-IR spectrum of $La_{0.90}Dy_{0.10}SrAl_3O_7$ nanophosphor, sintered at 550 ºC in the 4000-400 cm^{-1} range. IR bands in the region of 1000-400 cm^{-1} are associated to stretching and bending vibrations of AlO_4^{5-} group and other M-O bonds in the melilite lattice. The absorption peaks at 1630 cm^{-1} is assigned to bending vibrations of absorbing free H_2O while broad band in 2900 to 3700 cm^{-1} range can be attributed to stretching vibrations of O-H group in the lattice. The characteristic peak around 1384 cm^{-1} due to unreacted nitrates was not detected in the spectrum, which eventually confirm the XRD results that impurity free pure melilite $LaSrAl_3O_7$ structure was obtained at sintering temperature, 550 ºC.

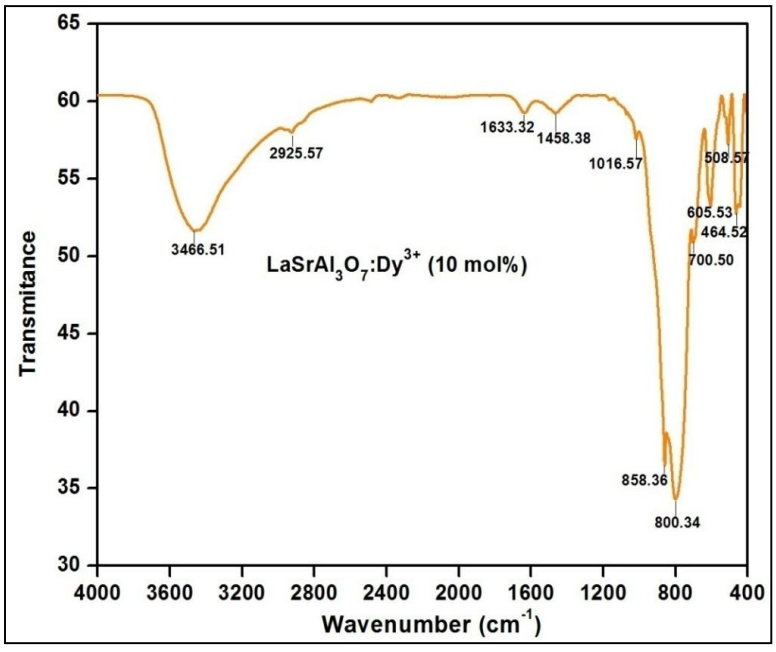

Fig 5: FT-IR spectrum of $La_{0.90}Dy_{0.10}SrAl_3O_7$ nanophosphor, sintered at 550 ºC in the 4000-400 cm^{-1} range.

The excitation spectrum of $La_{0.90}Dy_{0.10}SrAl_3O_7$ nanophosphor, sintered at 550 °C, recorded at 574 nm emission wavelength for the $^4F_{9/2} \rightarrow {}^6H_{13/2}$ transition is presented in Fig.6. It can be clearly seen that the excitation spectrum comprises of a series of sharp peaks between 300 and 500 nm attributed to characteristic 4*f* transitions of Dy^{3+} ions within its $4f^9$ configuration while host related or $Dy^{3+} \rightarrow O^{2-}$ charge transfer band has not been noticed in short wavelength region, suggesting weak interactions between dysprosium and oxygen in the melilite lattice.

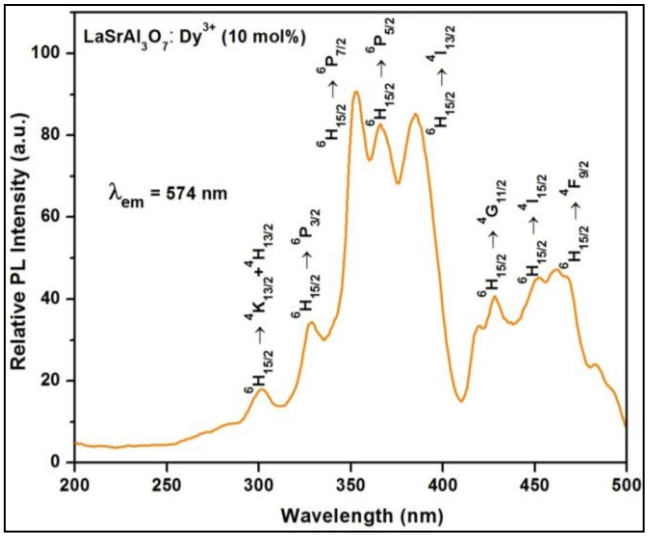

Fig 6: Photoluminescence excitation (PLE) spectrum of $La_{0.90}Dy_{0.10}SrAl_3O_7$ nanophosphor, sintered at 550 °C, monitored at 574 nm emission wavelength.

These excitation peaks in longer wavelength region are assigned to radiative transitions of Dy^{3+} ions from $^6H_{15/2}$ energy state to $^4K_{13/2}$ + $^4H_{13/2}$, $^6P_{3/2}$, $^6P_{7/2}$, $^6P_{5/2}$, $^4I_{13/2}$, $^4G_{11/2}$, $^4I_{15/2}$ and $^4F_{9/2}$ at 301 nm, 328 nm, 352 nm, 366 nm, 384 nm, 428 nm, 451 nm and 467 nm respectively in $LaSrAl_3O_7$ lattice [28-29]. The emission spectra of $La_{0.90}Dy_{0.10}SrAl_3O_7$ nanophosphor as-synthesized and sintered at 550 °C, recorded with 352 nm excitation wavelength for $^6H_{15/2} \rightarrow {}^6P_{7/2}$ in the range of 400-650 nm is shown in Fig.7. The spectra exhibit two main emission; blue emission centered at 478 nm in the 450-500 nm region and yellow emission centered at 574 nm in the range of 550-600 nm [30]. The blue emission belongs to the magnetic allowed dipole ($^4F_{9/2} \rightarrow {}^6H_{15/2}$) transitions of the Dy^{3+} ions which hardly influenced by the crystal field strength around dysprosium ions while yellow emission corresponds to forced electric allowed ($^4F_{9/2} \rightarrow {}^6H_{13/2}$) transitions with selection rule $\Delta J = 2$, being hypersensitive strongly affected by the outside environment. If Dy^{3+} ions are located at high symmetry site with an inversion centre, the $^4F_{9/2} \rightarrow {}^6H_{15/2}$ transition should be dominant; otherwise in a low symmetry site with no inversion centre, the hypersensitive $^4F_{9/2} \rightarrow {}^6H_{13/2}$ transition will be prominent in the emission spectra [4]. As per the crystal structure principle, Dy^{3+} ions may easily enter into the low symmetry sites of La^{3+} ions (C_s) in the $LaSrAl_3O_7$ structure on the basis of similar valence state and smaller ionic radii that of La^{3+}, hence for the both $La_{0.90}Dy_{0.10}SrAl_3O_7$ nanophosphors forced electric transition (yellow emission) found to be stronger than magnetic dipole transition (blue emission) as clearly visible in Fig.7. In both samples, sintering do not induce any significant change in the shape and positions of emission peaks although a slight increase in the intensity of as-synthesized $La_{0.90}Dy_{0.10}SrAl_3O_7$ nanophosphor was observed at higher temperature due to improvement in crystallinity.

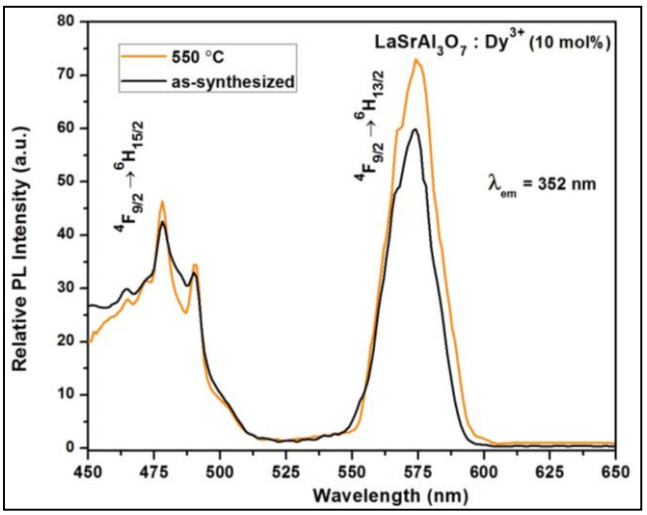

Fig 7: Photoluminescence (PL) spectra of $La_{0.90}Dy_{0.10}SrAl_3O_7$ nanophosphor as-synthesized and sintered at 550 °C, monitored with 352 nm excitation wavelength.

The emission spectra of $La_{1-x}Dy_xSrAl_3O_7$, where x = 1 to 15 mol% nanophosphors sintered at 550 °C, recorded at 352 nm as excitation wavelength are depicted in Fig. 8. For all $La_{1-x}Dy_xSrAl_3O_7$ powders, the spectra are dominated by hypersensitive yellow ($^4F_{9/2} \rightarrow {}^6H_{13/2}$) emission of dysprosium ions. The ratio of yellow to blue emission can be used as a spectroscopic probe to measure the degree of distortion of luminescent center from the inversion symmetry in the host. The value of Y/B emission ratio for different dysprosium contents in $La_{1-x}SrAl_3O_7$ powders has come out to be nearly 1.5, indicating that crystal field symmetry of Dy^{3+} ions in $LaSrAl_3O_7$ host does not vary with dopant concentration.

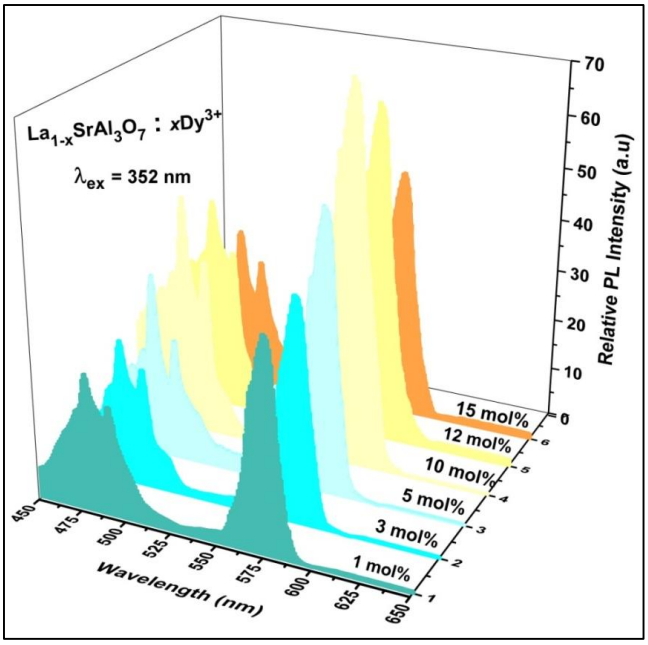

Fig 8: Photoluminescence (PL) spectra of $La_{1-x}Dy_xSrAl_3O_7$, where x = 1 to 15 mol% nanophosphors sintered at 550 °C, recorded at 352 nm as excitation wavelength.

It has been seen that emission intensity due to both transitions increases with the increasing Dy^{3+} ions concentration, and

maximum intensity approaches at 10 mol% of dysprosium contents, then the intensity decreased due to concentration quenching phenomenon. The possible explanation of this luminescence quenching behavior is the non-radiative energy transfer from $^4F_{9/2}$ state of Dy^{3+} ions via cross-relaxation process between two neighboring luminescent centers i.e. $^4F_{9/2}$ (Dy^{3+}) + $^6H_{15/2}$ (Dy^{3+}) → $^4F_{9/2}$/$^6H_{7/2}$ (Dy^{3+}) + $^6F_{3/2}$ (Dy^{3+}) [14]. The respective luminescence decay curves for $La_{1-x}Dy_xSrAl_3O_7$ nanophosphors at different Dy^{3+} ions concentrations corresponding to yellow emission ($^4F_{9/2}$ → $^6H_{13/2}$) at 574 nm, recorded at λ_{ex} = 352 nm are presented in Fig. 9. The decay curves corresponding to all dysprosium ion contents can be well fitted into single exponential functions, represented by the equation $I = I_0 \exp(-t/\tau)$, where τ is the radiative decay time, I and I_0 are the luminescence intensities at time t and 0, respectively.

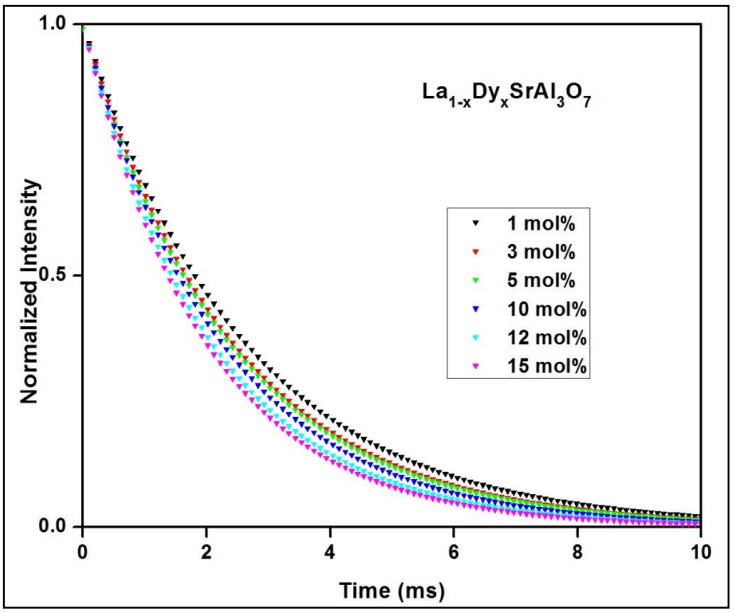

Fig 8: Decay curves of $La_{1-x}Dy_xSrAl_3O_7$, where x = 1 to 15 mol% nanophosphors sintered at 550 °C, recorded at λ_{ex} = 352 nm and λ_{em} = 574 nm.

It shows Dy^{3+} ions senses homogenous senses crystal field environment in $LaSrAl_3O_7$ lattice at different doping concentrations. The lifetimes determined are 1.98 ms, 1.65 ms, 1.62 ms, 1.44 ms, 1.33 ms and 1.28 ms for 1, 3, 5, 10, 12 and 15 mol% of Dy^{3+} ions, respectively in $La_{1-x}SrAl_3O_7$ nanophosphors. As stated earlier, shape of emission curves and Y/B ratio does not vary much over the range of dysprosium contents in $LaSrAl_3O_7$, hence the Commission International De I'Eclairage chromaticity coordinates corresponding to different concentrations of dysprosium fall in white region. At optimized concentration i.e $La_{0.90}Dy_{0.10}SrAl_3O_7$ nanophosphor, sintered at 550 °C exhibits color coordinates of x =0.332 and y = 0.351 quite close to other standard color systems such as NTSC (0.3101, 0.3162), PAL/SECAM/HDTV (0.3127, 0.329), ProPhoto/Color Match (0.3457, 0.3585) and CIE white light point (0.33, 0.33) as shown in Fig. 9.

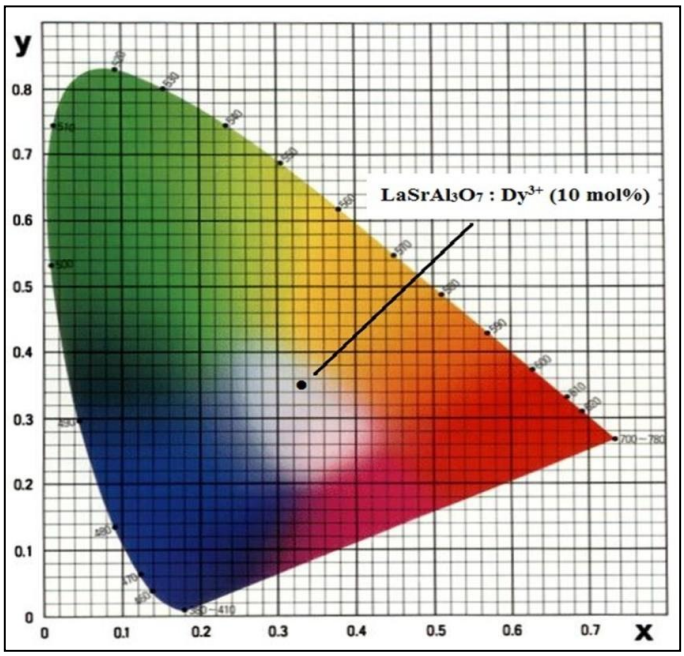

Fig 9: CIE color coordinates of $La_{0.90}Dy_{0.10}SrAl_3O_7$ nanophosphor sintered at 550 °C, monitored at λ_{ex} = 352 nm and λ_{em} = 574 nm.

Conclusion

In summary, low temperature solution combustion process has been successfully exploited to synthesize white light-emitting $LaSrAl_3O_7$: Dy^{3+} nanophosphors. XRD patterns demonstrated that single melilite phased nanophosphors could be readily obtained at 550 ºC. Morphological studies show that crystalline particles are uniform and tetragonal shaped having particle size in nano-regime. The emission spectra show strong white light emission (0.332, 0.351) attributed to characteristics yellow emission ($^4F_{9/2} \rightarrow {}^6H_{13/2}$) and blue emission ($^4F_{9/2} \rightarrow {}^6H_{15/2}$) of Dy^{3+} ions under excitation at 352 nm ($^6H_{15/2} \rightarrow {}^6P_{7/2}$). Dominant yellow emission due to hypersensitive $^4F_{9/2} \rightarrow {}^6H_{13/2}$ confirmed that Dy^{3+} ions occupied low symmetry La^{3+} sites in the melilite host. The dependence of the emission intensity of $La_{1-x}Dy_xSrAl_3O_7$ nanophosphors on the *x* value has also been investigated and found to be maximum at 10 mol% of dysprosium ions. Thus, the white light emission and easy synthetic method make this melilite nanophosphor suitable for LEDs application.

References

1. Zhang X, Seo HJ. Luminescence properties of novel Sm^{3+}, Dy^{3+} doped $LaMoO_6$ phosphors. Journal of Alloys and Compounds. 2011; 509:2007-2010.
2. Sharma G, Lochab SP, Singh N. Luminescence properties of CaS: Ce, Sm nanophosphors, Physics B. 2011; 406:2013-2017.
3. Dhananjaya N, Nagabhushana H, Nagabhushana BM, Chakradhar RPS, Shivakumara C, Rudraswamy B. Synthesis, characterization and photoluminescence properties of Gd_2O_3 :Eu^{3+} nanophosphors prepared by solution combustion method, Physics B. 2010; 405:3795-3799.
4. Rama Raju GS, Jung HC, Park JY, Kanamadi CM, Moon BY, Jeong JH *et al*. Synthesis and luminescent properties of Dy^{3+}: GAG nanophosphors. Journal of Alloys and Compounds. 2009; 481:730-734.
5. Khatkar SP, Han SD, Taxak VB, Sharma G, Kumar D. Synthesis and luminescent properties of $CaIn_2O_4$: xTb^{3+} nanocrystals, Current Applied Physics. 2006; 6S1:e192-e194.
6. Ayvacikli M, Ege A, Can N. Radioluminescence of $SrAl_2O_4$: Ln^{3+} (Ln = Eu, Sm, Dy) phosphor ceramic, Optical Materials, 2011; 34:138-142.
7. Shang Y, Yang P, Wang W, Wang Y, Niu N, Gai SS *et al*. Sol-gel preparation and characterization of uniform core-shell structured $LaInO_3$: Sm^{3+}/ Tb^{3+} @ SiO_2 phosphors. Journal of Alloys and Compounds. 2011; 509:837-844.
8. Jacobsohn LG, Bennett BL, Muenchausen RE, Smith JF, Cooke DW. Luminescent properties of nanophosphors, Radiation Measurements, 2007; 42:675-678.
9. Kumar RGA, Hata S, Ikeda K-I, Gopchandran KG. Influence of metal ion concentration in glycol mediated synthesis of Gd_2O_3: Eu^{3+} nanophosphor, Ceramic International. 2014; 40:2915-2926.
10. Rama Raju GS, Park JY, Jung HC, Moon BK, Jeong JH, Kim JH. Luminescence properties of Dy^{3+}: $GdAlO_3$ nanopowder phosphors, Current Applied Physics. 2009; 9:e92-e95.
11. Han SD, Khatkar SP, Taxak V, Sharma G, Kumar D. Synthesis, luminescence and effect of heat treatment on the properties of Dy^{3+} doped YVO_4 phosphor, Material Science & Engineering B, 2006; 129:126-130.
12. Kesavulu CR, Jayasankar CK. White light emission in Dy^{3+} doped lead flurophosphate glasses, Material Chemistry Physics, 2011; 130:1078-1085.
13. Diaz-Torres LA, Rosa EDL, Salas P, Romero VH, Angeles-Chavez A. Efficient photoluminescence of Dy^{3+} at low concentrations on nanocrystalline ZrO_2. Journal of Solid State Chemistry. 2008; 181:75-80.
14. Kale MA, Joshi CP, Moharil SV, Muthal PL, Dhopte SM. Luminescence in $LaCaAl_3O_7$ prepared by combustion synthesis. Journal of Luminescence. 2008; 128:1225-1228.
15. Singh V, Kumar VVRK, Chakradhar RPS, Kwak HY. Synthesis, characterization and photoluminescence of Eu^{3+}, Ce^{3+} co-doped $CaLaAl_3O_7$ phosphors, Philosophical Magazine, 2010; 90:3095-3105.
16. Sheetal VB, Taxak Mandeep, Khatkar SP. Synthesis, characterization and luminescent properties of Eu/Tb-doped $LaSrAl_3O_7$. Journal of Alloys and Compounds. 2013; 549:135-140.
17. Bao A, Yang H, Tao C. Synthesis and luminescent properties of nanoparticles $LaSrAl_3O_7$: Eu, Tb, Current Applied Physics, 2009; 9:1252-1256.
18. Singh V, Rai VK, Shamery KA, Nordmann J, Hasse M. NIR to visible upconversion in Er^{3+}/ Yb^{3+} co-doped $CaYAl_3O_7$ phosphor obtained by solution combustion process. Journal of Luminescence. 2011; 131:2679-2682.
19. Zhou L, Choy WCH, Shi J, Gong M, Liang H, Yuk TI. Synthesis, vaccum ultraviolet and near ultraviolet-excited luminescent properties of $GdCaAl_3O_7$: RE^{3+} (RE = Eu, Tb). Journal of Solid State Chemistry. 2005; 178:3004-3009.
20. Singh V, Watanabe S, Gundurao TK, Kwak HY. Synthesis, characterization, luminescence and defect centres in $CaYAl_3O_7$: Eu^{3+}. Journal of Fluorescence. 2011; 21:313-320.
21. Kubota S, Izumi M, Yamane H, Shimada M. Luminescence of Eu^{3+}, Tb^{3+} and Tm^{3+} in $SrLaGa_3O_7$, Journal of Alloys and Compounds. 1999; 283:95-101.
22. Kodama N, Tanii Y, Yamaga M. Optical properties of long-lasting phosphorescent crystals Ce^{3+} doped $Ca_2Al_2SiO_7$ and $CaYAl_3O_7$. Journal of Luminescence. 2000; 87:1076-1078.
23. Zhang X, Zhang J, Liang L, Su Q. Luminescence of $SrGdGa_3O_7$: RE^{3+} (RE = Eu, Tb) phosphors and energy transfer from Gd^{3+} to RE^{3+}, Material Research Bulletin, 2005; 40:281-288.
24. Karbowiak M, Gnutek P, Rudowicz C, Romanowski WR. Crystal-field analysis for RE^{3+} ions in laser materials: II. Absorption spectra and energy levels calculations for Nd^{3+} ions doped into $SrLaGa_3O_7$ and $BaLaGa_3O_7$ crystals and Tm^{3+} ions in $SrGdGa_3O_7$, Chemistry Physics, 2011; 387:69-78.
25. Romanowski WR, Golab S, Pisarski WA, Dzik GD, Berkowski M, Pajaczkowska A. Growth and characterization of new disordered crystals for the design of all solid state lasers. International Journal of Electronics. 1996; 81:457-465.
26. Bandi VR, Grandhe BK, Jang K, Lee H-S, Shin D-S, Yi S-S *et al*. Citrate based sol-gel synthesis and luminescence characteristics of $CaLa_2ZnO_5$: Eu^{3+} phosphors for blue LED excited white LEDs. Journals of Alloys and Compounds. 2012; 512:264-269.
27. Ekambaram S, Maaza M, Patil KC. Synthesis of lamp phosphors: facile combustion approach. Journal of Alloys

and Compounds. 2005; 93:81-92.
28. Liang C-H, Teoh L-G, Liu KT, Chang Y-S. Near white light emission of BaY_2ZnO_5 doped with Dy^{3+} ions. Journal Alloys and Compounds. 2012; 517:9-13.
29. Tian B, Chen B, Tian Y, Sun J, Li X, Zhang J *et al*. Concentration and temperature quenching mechanisms of Dy^{3+} luminescence in $BaGd_2ZnO_5$ phosphors. Journal of Physics Chemistry Solids. 2012; 73:1314-1319.
30. Yan B, Su X-Q. Chemical co-precipitation synthesis of luminescent $Bi_xY_{1-x}VO_4$: RE (RE = Eu^{3+}, Dy^{3+}, Er^{3+}) phosphors for hybrid precursors. Journal of Non-Crystalline Solids. 2006; 352:3275-3279.